Alberto Cini, Pierpaolo Ceci, Elisabetta Falvo, Dante Gatteschi and Maria Fittipaldi*

An EPR Study of Small Magnetic Nanoparticles

DOI 10.1515/zpch-2016-0846
Received July 1, 2016; accepted August 16, 2016

Abstract: Magnetic nanoparticles (MNPs) of spinel type iron oxide (of approximately 4 nm) mineralized inside the internal cavity of a mini ferritin-type protein have been investigated by means of electron magnetic resonance (EMR) spectroscopy. EMR measurements have been recorded at different temperatures in perpendicular and parallel configurations. The spectra have been interpreted using an approach based on the giant spin model. We confirm the quantum behavior of the MNPs, moreover, the thermal evolution of the spin system in terms of population of excited spin states is showed.

Keywords: electron paramagnetic resonance; magnetic nanoparticles; quantum behavior.

Dedicated to: Professor Dr. Kev Salikhov in occasion of his 80th birthday for his outstanding contribution in the field of magnetic resonance.

1 Introduction

Nanomagnetic systems have gained great interest in recent years due to their potentialities both in fundamental science [1, 2] and in many technological fields [3–14]. This interest is driven by the emergence of new properties which are reliant on their reduced dimensions. In particular, two classes of zero-dimensional magnetic objects can be recognized: magnetic nanoparticles (MNPs) and molecular nanomagnets (MNMs). Generally, these magnetic systems have been characterized

***Corresponding author: Maria Fittipaldi,** INSTM and Department of Physics and Astronomy, University of Florence, via Sansone 1, 50019 Sesto Fiorentino, Italy, E-mail: maria.fittipaldi@unifi.it
Alberto Cini: INSTM and Department of Physics and Astronomy, University of Florence, via Sansone 1, 50019 Sesto Fiorentino, Italy
Pierpaolo Ceci and Elisabetta Falvo: Institute of Molecular Biology and Pathology, CNR – National Research Council of Italy, 00185 Rome, Italy
Dante Gatteschi: INSTM and Department of Chemistry "U. Schiff", University of Florence, via della Lastruccia, 3-13 50019 Sesto Fiorentino, Italy

and studied in two different ways: MNPs are obtained by a top down approach and are theoretically described by classical mechanics; MNMs are instead obtained by a bottom up approach and their behavior interpreted with the aid of quantum mechanics. Recently the need for a unified view of the two magnetic objects has been proposed, justified by the fact that they have reached the same dimensions, with the aim to get a deeper understanding of their properties [1, 15]. Evidence in this direction has been provided by electron magnetic resonance (EMR) studies [16–19]. In particular, signatures of the discrete nature of the energy levels in MNPs have emerged, displaying the quantum nature of the system.

We have investigated MNPs of spinel type iron oxide of approximately 4 nm, mineralized in the internal cavity of the Dps protein (a protein belonging to the ferritin family). In particular, we utilized the Dps protein from *Listeria innocua* (LiDps) as a protein cage system that differs from ferritins in its smaller size (9 nm outer and 4.5 nm inner diameter as compared to 12 and 8 nm, respectively). Using a previously exploited approach [16], we were able to control the size and the iron oxide phase of the MNPs. The MNPs thus formed inside the protein cages contain at least 400 Fe ions, in the form of maghemite/magnetite.

The quantum behavior of these MNPs has been investigated with EMR spectroscopy. EMR spectra have been recorded at different temperatures in two different configurations, parallel and perpendicular, i.e. with the B_1 field of the microwave radiation parallel and perpendicular to the external B_0 field. The allowed transitions between the total spin projections have different selection rules in the two realized configurations: these alternative measurements are thus a way to sense and address the quantum nature of the system.

To extract useful information from the EMR data we compared them with simulated spectra of MNPs. Simulations have been realized following an approach based on the giant spin model. This approach has been extensively used for MNMs to describe the interaction of their spin ground state with the external magnetic field [20–24]. However, considering the MNPs as an ensemble of hundreds of Fe(III) ions, each of spin 5/2, and conjecturing a ferromagnetic coupling between them, a rough estimation of the total spin of the system would give at least a value of 1000. This would reflect on a great dimension of the associated Hilbert space. Then we decided to follow a simplified approach based on the definition of an effective lower spin for the system, and accordingly spin Hamiltonian and experimental parameters. This approach has already been successfully used for the interpretation of EMR spectra relative to MNPs mineralized inside the ferritin protein [19].

In this work we confirm the usefulness of this approach and we take advantage of it to study in detail the thermal evolution of the spin state of the system. We show that the temperature behavior of the spectra arises from the thermal population of excited spin states.

2 Materials and methods

2.1 EMR spectroscopy

X-band EMR measurements were performed using the 9 GHz Bruker Elexys E500 instrument (Bruker, Rheinstetten, Germany) equipped with a microwave frequency counter. An Oxford Instruments ESR 900 continuous He flow cryostat was used to obtain low temperatures. EPR spectra were acquired using a field modulation of 100 kHz and 5 G, and a microwave power of 26 μW for the perpendicular configuration and 21 mW for the parallel configuration. The ER 4116DM EPR-resonator (Bruker, Rheinstetten, Germany) was used for the measurements.

2.2 MNP synthesis in LiDps proteins

Apo-LiDps proteins were expressed and purified as reported elsewhere [17, 25]. MNPs were encapsulated inside the LiDps nanocage as previously reported by ourselves, with minor modifications [16]. Iron incorporation experiments were carried out at 65 °C on 1 mg/mL LiDps samples in 5 mM Hepes-NaOH (Sigma Aldrich, Italy) at a pH of 8.5. Solutions of iron(II) sulfate heptahydrate (Sigma Aldrich, Italy) dissolved in 0.5 mM HCl were used as an iron source. During the course of the experiment, the reaction vessel was kept at 65 °C under a positive N_2 pressure, and the pH was maintained dynamically at 8.5 with 100 mM NaOH by means of an automatic titrator (TITRINO, Metrohm AG). Solutions of $FeSO_4$ (15 mM) and H_2O_2 (5 mM) were added simultaneously and at a constant rate (0.5 mL/min) using two peristaltic pumps. The iron loading factor was 450 Fe(II)/protein. Any aggregate of protein and iron oxides produced during MNP formation were removed by centrifugation at 16,000 rpm for 45 min at 4 °C and by filtration through 0.2-μm filters. MNPs were purified by size exclusion chromatography (SEC) using a Superose 6 gel-filtration column equilibrated with 0.15 M HEPES-NaOH buffer at pH 7.8. The protein and iron contents in the samples containing MNPs were assessed by means of native electrophoresis on 1% agarose gels and of the ferrozine method as described in Ceci et al. [17].

3 Results

EMR spectra of MNPs internalized inside LiDps proteins have been acquired at X-band in both perpendicular and parallel configurations for various

temperatures comprised between 150 K and 5 K. These measurements are reported in Figures 1 and 2, respectively. The spectrum measured at 150 K in the perpendicular configuration shows a resonance at a field B_0 of about 3400 G; this

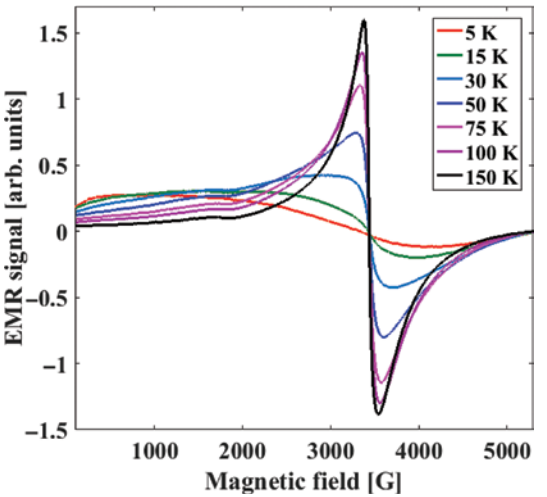

Fig. 1: EMR spectra of MNPs in LiDps proteins acquired at X-band in perpendicular configuration at various temperatures. The microwave frequency used was 9.64 GHz.

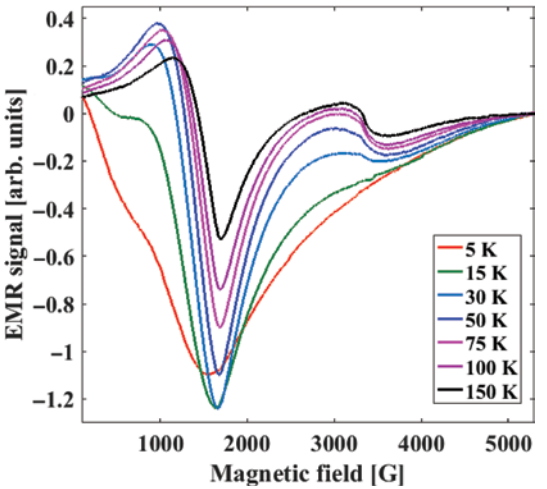

Fig. 2: EMR spectra of MNPs in LiDps proteins acquired at X-band in parallel configuration at various temperatures. The microwave frequency used was 9.40 GHz.

resonance becomes broader and shifts toward a lower value upon decreasing the temperature. It is also possible to observe at higher temperatures the presence of a band with a minor intensity at a field around half B_0. This band may be ascribed to 'partially' forbidden transitions between spin states with $\Delta M = \pm 2$, where M is the expectation value of $\hat{S}_z$ and S is the total spin of the MNP. This interpretation is confirmed by the spectra recorded in the parallel configuration: Figure 2 shows effectively an increase in the signal from the MNPs at $B_0/2$. Finally, as in the perpendicular case, the spectra become broader and shift to a minor field value upon lowering the temperature.

4 Theoretical model

In order to interpret the EMR spectra obtained for MNPs grown inside LiDps proteins, simulations have been performed for both configurations at every temperature. These simulations were based on the giant spin associated with the whole MNP. From previously reported data [16], the saturation magnetization (obtained at 1.8 K) and the anisotropy field B_a were found to be 59.7 emu g^{-1} and 0.3 T, respectively. The magnetic moment of each MNP can be estimated from the relation $\mu = M_S V_p$, where M_S is the volume magnetization and V_p the particle volume; for MNPs inside LiDps M_S is equal to 298.5 emu cm^{-3} (obtained assuming a density of 5 g cm^{-3} for maghemite or magnetite) and the particle radius is 1.7 nm.

With these data the relation $S = \frac{\mu}{g\mu_B}$ enables to evaluate the ground state spin value to be of the order of 300; moreover, using $D = -\frac{g\mu_B B_a}{2S}$, a D value of about –13 MHz (-4.3×10^{-4} cm^{-1}) is found.

Given these estimated S and D values, the huge dimension of the Hilbert space associated with the system prompted us to use a simplified simulation approach, employing an effective smaller spin value and, accordingly, effective spin Hamiltonian and experimental parameters, as successfully done in a preceding work on MNPs mineralized in the internal cavity of the ferritin protein [19]. Briefly, this model is based on the possibility to simulate the EMR spectrum of MNPs of spin S by means of an effective lower spin $S_{\text{eff}} = \frac{S}{n}$ (with n integer and positive). This assumption determines the necessity to also define an effective D value $D_{\text{eff}} = nD$ and an effective temperature $T_{\text{eff}} = \frac{T}{n}$ relied to the D value of the spin system and to the experimental temperature T, respectively. The spin Hamiltonian used for this system is then

$$H = \mu_B \hat{S}_{\text{eff}} \cdot g \cdot \vec{B} + \hat{S}_{\text{eff}} \cdot \hat{D}_{\text{eff}} \cdot \hat{S}_{\text{eff}} \quad (1)$$

where the first term is the Zeeman term and the second is the zero field splitting term.

To simulate the EMR spectra of the MNPs in LiDps, an effective spin of 10 has been chosen (i.e. $n = 30$), corresponding to a spin value of 300. However, the adoption of a corresponding $D_{\text{eff}} \sim -400$ MHz did not allow to obtain good simulations of the experimental spectra along all the temperature range and for both configurations. This was instead achieved by using two different effective spin states and correspondingly two distinct effective D values (D_1 and D_2). At each temperature, the corresponding simulated spectra were combined by means of two different temperature dependent weights ($\alpha(T)$ and $\beta(T)$) to reproduce the experimental one. Therefore, the simulated spectrum at temperature T was obtained as:

$$Spec(T) = \alpha(T) Spec1(S_1, D_1, T) + \beta(T) Spec2(S_2, D_2, T) \quad (2)$$

where $Spec1(S_1, D_1, T)$ and $Spec2(S_2, D_2, T)$ are the spectra simulated at fixed T with the D value D_1 and D_2, respectively, associated with the spin states S_1 and S_2.

With this strategy we take into account the effect of excited spin states in the EPR spectra, as these are expected to be lying very close to the ground spin state. The best simulations were achieved by using, for each configuration at each temperature, two spin states with $S_{\text{eff}} = 10$ and the same n value of 30 (one with a D value of –500 MHz and one with a D value of –200 MHz). Therefore, we have considered each experimental spectrum as resulting from the contributions of two equal spin states ($S = 300$), but having two different D values. In association with D_1 and D_2 we used two different strains on the D values (i.e. two different widths for the D distributions) $Dstrain_1 = 50$ MHz and $Dstrain_2 = 200$ MHz; these values are the same for every temperature and configuration (only in the perpendicular case at 5 K it was necessary to use a $Dstrain_1$ of 500 MHz and to also introduce a strain on E of 100 MHz). Moreover, for each temperature and configuration, the linewidths associated with the resonance of the two states have been varied. The spectra have been simulated with Easyspin [26].

The comparison between the experimental and the simulated spectra at each temperature for both configurations are reported in Figures 3 and 4 (the same images including also the contributions due to the S_1 and S_2 are reported in the Supplementary Info). Looking at the perpendicular case, at 150 K the agreement between the experimental data and the simulation is very good: the simulation shows the resonance at B_0 and also a resonance with lesser intensity at about $B_0/2$. This trend is well represented until 30 K, although there is an increasing discrepancy between the data and the simulations in the low field region. The agreement is poorer at 15 K and 5 K: however, the simulations still

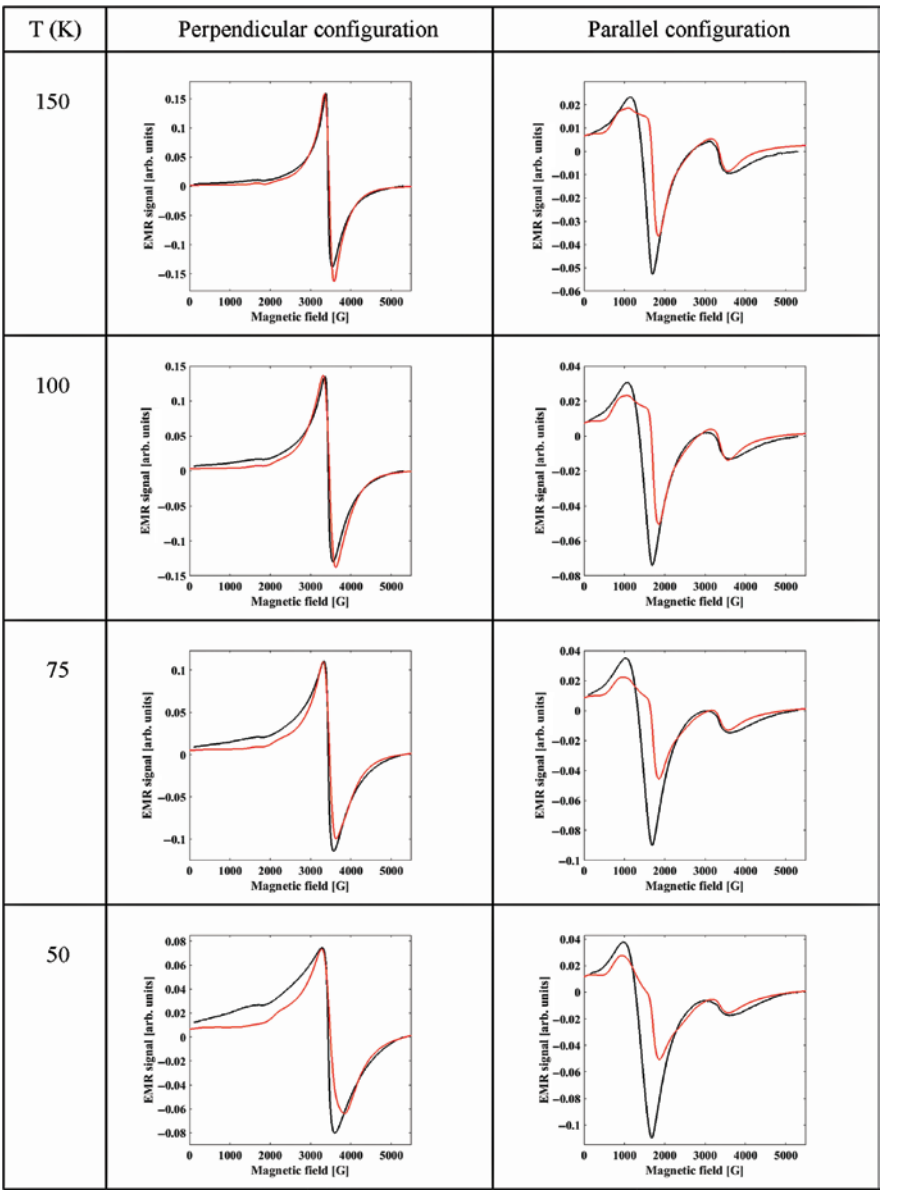

Fig. 3: Experimental EMR spectra (black line) acquired in the parallel and perpendicular configurations at 150 K, 100 K, 75 K and 50 K and corresponding simulations (red line). The simulated spectrum is the result of the combination between two systems with $S_{eff} = 10$ and different D values and linewidths.

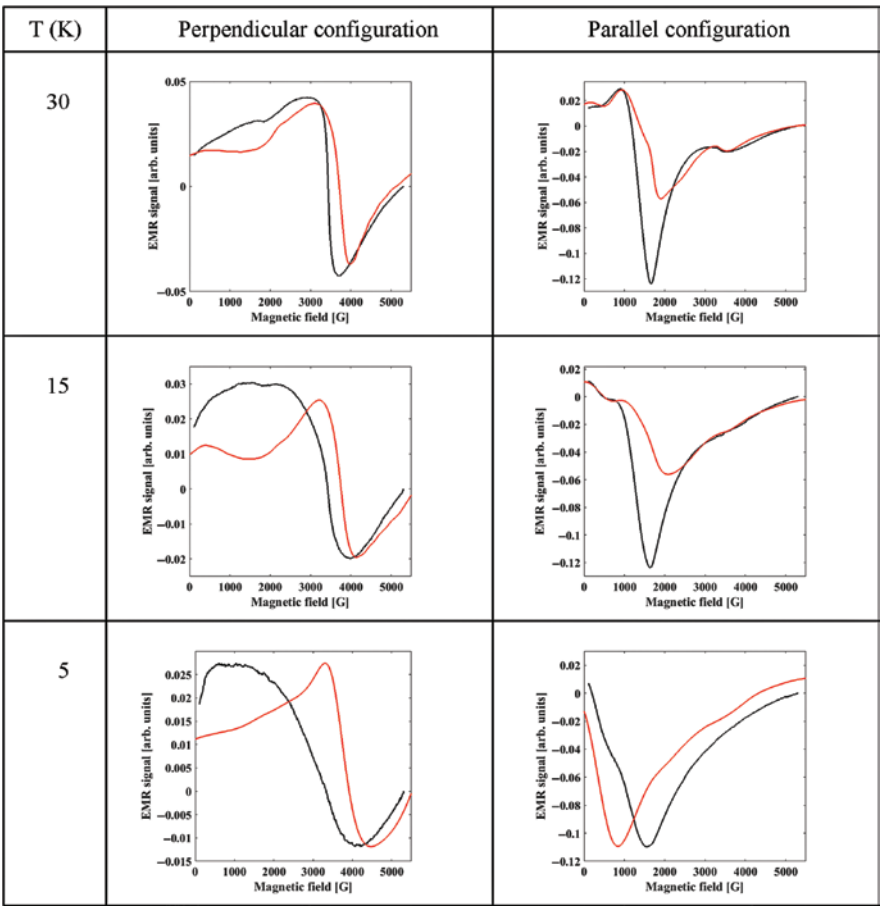

Fig. 4: Experimental EMR spectra (black line) acquired in the parallel and perpendicular configurations at 30 K, 15 K and 5 K and corresponding simulations (red line). The simulated spectrum is the result of the combination between two systems with $S_{eff} = 10$ and different D values and linewidths.

give the correct trend at high field. The situation is very similar in the parallel configuration: at 150 K the agreement is good, although the presence of a slight shift between the experimental spectrum and the simulation. Between 75 K and 15 K there is an increasing lack of intensity in the simulated data at low field, but the agreement remains acceptable. The measured spectrum is instead well reproduced at 5 K.

In Figure 5 the temperature dependence of the $\alpha(T)$ and $\beta(T)$ parameters used to combine the two spectra corresponding to the two S states (with two different

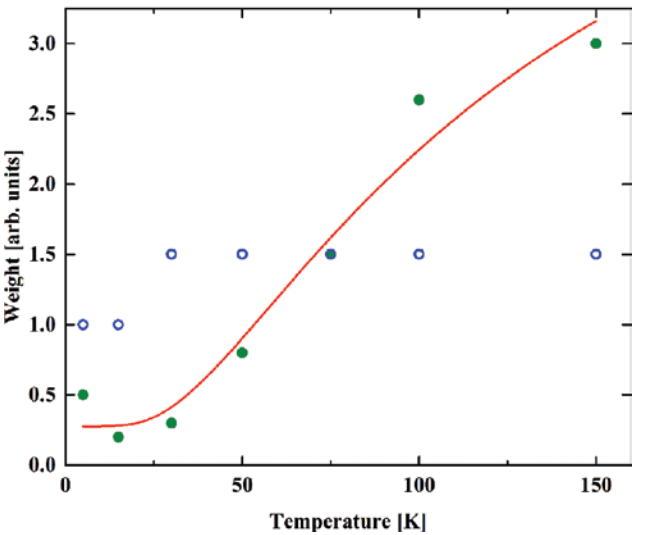

Fig. 5: Temperature dependence of the $\alpha(T)$ (blue circles) and $\beta(T)$ (green dots) parameters used to combine the simulated spectra relative to the S_1 and S_2 states. The red line is a fit of the $\beta(T)$ parameter by means of an exponential function.

D values) are reported. At each temperature, the same values were considered for both experimental configurations, perpendicular and parallel, respectively. In particular, while $\alpha(T)$ (the weight corresponding to the state with D_1=–500 MHz) remains practically constant, $\beta(T)$ (the weight corresponding to D_2=–200 MHz) decreases with the temperature. It is instructive to analyze the thermal evolution of the $\alpha(T)$ and $\beta(T)$ parameters. We fitted this behavior with an exponential function of the form $\beta(T) = a + be^{\left(-\frac{T_0}{T}\right)}$ (the fit is shown in Figure 5). The values for the fit parameters are: $a = 0.3 \pm 0.2$, $b = 6.2 \pm 1.3$, and $T_0 = (115 \pm 26)$ K.

Figure 6 reports the temperature dependence of the linewidths used for the simulation of the spectra for the two contributions for both configurations. These values differ between the two states and the two configurations, but have the same trend with the temperature: they increase upon lowering the temperature. Furthermore, while the linewidths corresponding to S_1 change little, the linewidths corresponding to S_2 show a great increase below 50 K.

In Figure 7 the temperature behavior of the double integral of the EMR spectra acquired in both experimental configurations are reported together with those obtained from the simulations. Although the trend is roughly reproduced for both configurations, the agreement is better at the highest temperatures. The very broad character of the spectra, especially at low temperatures, renders

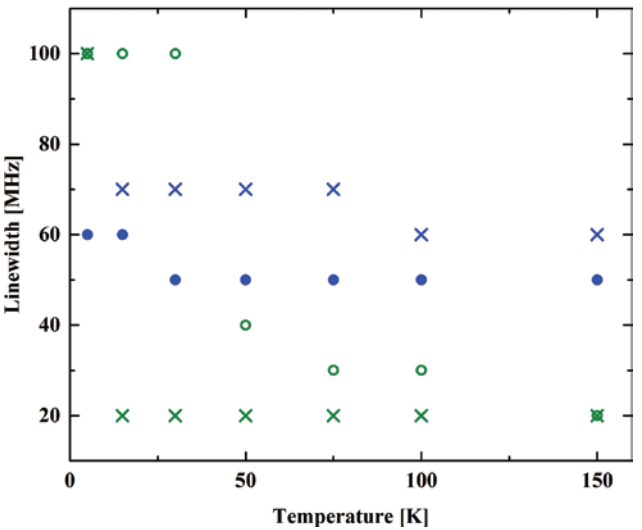

Fig. 6: Temperature dependence of the linewidths used for the spectra relative to S_1 (in blue) and S_2 (in green) in the perpendicular and the parallel configuration (dots and crosses, respectively).

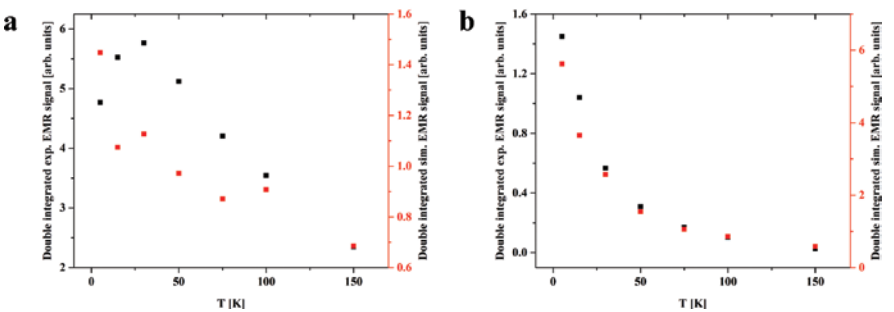

Fig. 7: Temperature dependence of the double integral of the experimental EMR spectra (black) acquired in both experimental configurations, perpendicular (a) and parallel (b), and of the simulated EMR spectra (red).

the evaluation of the double integral more problematic. Moreover, the discrepancy between the experimental and the simulated spectra is higher at lower temperatures. The maximum observed in the experimental data of Figure 7a, has been attributed to the blocking temperature relative to the experimental technique [27].

5 Discussion

EMR spectra of MNPs mineralized inside the LiDps protein have been acquired in perpendicular and parallel configurations for different temperatures from 150 K to 5 K. The spectra have been interpreted using a simplified version of the giant spin model. The key property of this simplified view is the substitution of the huge spin value associated to the system with a lower effective spin value; in this case we used an effective spin of 10 in place of an estimated spin value of 300 for each MNP inside the LiDps protein. In a preceding work on MNPs mineralized in the ferritin protein [19] we used the same approach in conjunction with the inclusion of a temperature dependent parameter exemplifying a non isotropic distribution of easy axes: the spectra were then simulated after a discretization over the angle between the easy axis of the ZFS tensor and the direction of the external magnetic field. The introduction of that temperature dependent parameter was correlated with the fact that the spin state describing the system is not constant with the temperature.

Here, we made complete simulations, for all the experimental temperatures and in both experimental configurations, by assuming a random orientation of the easy axes of the MNPs in the frozen suspension, in the attempt to better describe the thermal evolution of the spin states of the system. We encountered the necessity to simulate the system of the MNPs as the combination of two subsystems having the same effective spin, but different D values (and different corresponding strain over them). The combination of the two spin states resulted in being temperature dependent, therefore, excluding the possibility that this describes a possible heterogeneity of the sample. The same combination of these two subsystems allows to simulate the spectra acquired for the perpendicular and the parallel configurations. We want to emphasize the fact that the use of the same parameters to reproduce data acquired with two different experimental configurations is a test for the confidence of the parameters found, keeping in mind that the system is far more complicated, and the approach followed gives a simplified and fair description of its behavior. In summary, the necessity to combine two different subsystems is a way to take into account the thermal population of spin states of MNPs. The lesson we learn from MNMs is that, by increasing the number of magnetic centers, the excited spin states become closer in energy with respect to the fundamental spin state, therefore they have to be considered in the thermal evolution of the EMR spectra (see [28] and references therein). The inclusion of other terms in the spin Hamiltonian, although possible, is in our opinion of secondary importance with respect to the inclusion of excited spin states for two reasons. First, we recall that for the MNM Fe_{19} the separation between the first excited spin state and the ground spin state is of 8 K, and this

is expected to decrease by increasing the number of magnetic centers, e.g. for Fe_8 it is 24 K (see [28] and references therein). Second, from the angular dependence of EMR spectra acquired in perpendicular orientation for a solution of MNPs frozen in an external magnetic field [16, 27] an axial anisotropy is derived for the resonance position of the main resonance, giving no indication of higher order contributions to the spin Hamiltonian.

The temperature T_0, obtained from the fit of the $\beta(T)$ value, gives an indication of the energy separation between the energy levels of the spin states considered. The value we find from the fit is rather above the expected one [15, 16]. However, we consider this value affected by a decreasing quality of our simulations at low temperature: the discrepancy between measured and simulated spectra in this thermal range may determine its overestimation.

In this work, EMR measurements in X-band are reported. In this band the Zeeman interaction is of the same order of magnitude of the ZFS interaction: the ratio between the transitions at $B_0/2$ and B_0 is expected to strongly decrease by increasing the external field value and this has been already reported by comparing X-band and W-band measurements [16], again stressing on the quantum nature of the system.

In conclusion, we have demonstrated the possibility to efficiently simulate EPR spectra of MNPs with a modified version of the giant spin model; with the proposed approximation we can simulate EMR spectra of huge S values, describing the system with same spin Hamiltonian parameters in both configurations for a wide range of temperatures. Finally, this description enables to evidence the quantum behavior of the MNPs.

Acknowledgements: Dr. Silvia Sottini is acknowledged for her help during the EMR measurements.

References

1. M. Fittipaldi, L. Sorace, A.-L. Barra, C. Sangregorio, Phys. Chem. Chem. Phys. **11** (2009) 6553.
2. W. Wernsdorfer, Adv. Chem. Phys. **118** (2001) 99.
3. A.-H. Lu, E. L. Salabas, F. Schüth, Angew. Chemie Int. Ed. **46** (2007) 1222.
4. A.-H. Lu, W. Schmidt, N. Matoussevitch, H. Bönnemann, B. Spliethoff, B. Tesche, E. Bill, W. Kiefer and F. Schüth, Angew. Chemie – Int. Ed. **43** (2004) 4303.
5. T. Hyeon, Chem. Commun. **271** (2003) 927.
6. T. Shinjo (Ed.), Nanomagnetism and Spintronics, Elsevier, Amsterdam, The Netherlands (2009).
7. S. Laurent, D. Forge, M. Port, A. Roch, C. Robic, L. Vander Elst, R. N. Muller, Chem. Rev. **108** (2008) 2064.

8. W. Andrä, H. Nowak (Ed.), Magnetism in Medicine: A Handbook, Wiley – VCH, Weinheim, Germany (2007).
9. S. Chikazumi, S. Taketomi, M. Ukita, M. Mizukami, H. Miyajima, M. Setogawa, Y. Kurihara, J. Magn. Magn. Mater. **65** (1987) 245.
10. A. K. Gupta, M. Gupta, Biomaterials **26** (2005) 3995.
11. Q. A. Pankhurst, J. Connolly, S. K. Jones, J. Dobson, J. Phys. D. Appl. Phys. **36** (2003) R167.
12. D. W. Elliott, W. Zhang, Environ. Sci. Technol. **35** (2001) 4922.
13. M. Takafuji, S. Ide, H. Ihara, Z. Xu, Chem. Mater. **16** (2004) 1977.
14. E. Fantechi, C. Innocenti, M. Zanardelli, M. Fittipaldi, E. Falvo, M. Carbo, V. Shullani, L. Cesare Mannelli, C. Ghelardini, A. M. Ferretti, A. Ponti, C. Sangregorio, P. Ceci, ACS Nano **8** (2014) 4705.
15. D. Gatteschi, M. Fittipaldi, C. Sangregorio, L. Sorace, Angew. Chemie Int. Ed. **51** (2012) 4792.
16. M. Fittipaldi, C. Innocenti, P. Ceci, C. Sangregorio, L. Castelli, L. Sorace, D. Gatteschi, Phys. Rev. B Condens. Matter Mater. Phys. **83** (2011) 104409.
17. P. Ceci, E. Chiancone, O. Kasyutich, G. Bellapadrona, L. Castelli, M. Fittipaldi, D. Gatteschi, C. Innocenti, C. Sangregorio, Chem. – A Eur. J. **16** (2010) 709.
18. N. Noginova, T. Weaver, E. P. Giannelis, A. B. Bourlinos, V. A. Atsarkin, V. V. Demidov, Phys. Rev. B – Condens. Matter Mater. Phys. **77** (2008) 1.
19. M. Fittipaldi, R. Mercatelli, S. Sottini, P. Ceci, E. Falvo, D. Gatteschi, Phys. Chem. Chem. Phys. **18** (2016) 3591.
20. A.-L. Barra, L.-C. Brunel, D. Gatteschi, L. Pardi, R. Sessoli, Acc. Chem. Res. **31** (1998) 460.
21. D. Gatteschi, A. L. Barra, A. Caneschi, A. Cornia, R. Sessoli, L. Sorace, Coord. Chem. Rev. **250** (2006) 1514.
22. E. J. L. McInnes, Spectroscopy of Single-molecule Magnets, Springer, Berlin, Germany (2006).
23. R. S. Edwards, S. Maccagnano, E. C. Yang, S. Hill, W. Wernsdorfer, D. Hendrickson, G. Christou, J. Appl. Phys. **93** (2003) 7807.
24. S. Hill, S. Maccagnano, K. Park, R. M. Achey, J. M. North, N. S. Dalal, Phys. Rev. B **65** (2002) 224410.
25. O. Kasyutich, A. Ilari, A. Fiorillo, D. Tatchev, A. Hoell, P. Ceci, J. Am. Chem. Soc. **132** (2010) 3621.
26. S. Stoll, A. Schweiger, J. Magn. Reson. **178** (2006) 42.
27. F. Moro, R. De Miguel, M. Jenkins, C. Gómez-Moreno, D. Sells, F. Tuna, E. J. L. McInnes, A. Lostao, F. Luis, J. Van Slageren, J. Magn. Magn. Mater. **361** (2014) 188.
28. L. Castelli, M. Fittipaldi, A. K. Powell, D. Gatteschi, L. Sorace, Dalton Trans. **40** (2011) 8145.